

Supplementary Information

Seed Crystal Free Growth of High-quality Double Cation – Double Halide Perovskite Single Crystals for Optoelectronic Applications

*Julian Höcker¹, Mehmet Ozcan², Sebastian Hammer¹, Mathias Fischer¹, Benedikt Bichler²,
Melina Armer¹, Philipp Rieder¹, Volker Drach¹, Jens Pflaum^{1,3}, Bert Nickel², and Vladimir
Dyakonov^{1,3}*

¹ Experimental Physics VI, Am Hubland, Julius Maximilian University of Würzburg, Germany;

² Soft Condensed Matter Group, Geschwister-Scholl-Platz 1, Ludwig Maximilian University of
München, 80539 München, Germany;

³ Bavarian Center for Applied Energy Research (ZAE Bayern), Magdalene Schoch Str. 3, 97074
Würzburg, Germany

Table of Contents

Figure S1. Setup of RFCM.	S3
Figure S2. XRF results of the $(\text{FAPbI}_3)_{0.9}(\text{MAPbBr}_3)_{0.1}$ crystal powder and crystal surface	S4
Table S1. Evaluation of XRF measurements	S4
Figure S3. Measured and simulated XRD patterns of the $(\text{FAPbI}_3)_{0.9}(\text{MAPbBr}_3)_{0.1}$ powder.....	S5
Table S2. Evaluation of the XRD fitting data of $(\text{FAPbI}_3)_{0.9}(\text{MAPbBr}_3)_{0.1}$	S5
Figure S4. Long-term stability XRD – test over one year.....	S6
Figure S5. Measured and simulated XRD patterns of the FAPbI_3 crystal powder	S7
Table S3. Evaluation of the XRD fitting data of $\alpha\text{-FAPbI}_3$	S7
Figure S6. Comparison of out-of-plane XRD measurements of the crystal bulk.....	S8
Figure S7. Sample holder data subtracted XRD data (in reflection geometry)	S9
Figure S8. XRD data (in reflection geometry) of $(\text{FAPbI}_3)_{0.9}(\text{MAPbBr}_3)_{0.1}$ single crystal.....	S9
Figure S9. Measured and simulated XRD patterns of the MAPbBr_3 crystal powder	S10
Table S4. Evaluation of the XRD fitting data of MAPbBr_3	S10
Figure S10. I-V curves of the $(\text{FAPbI}_3)_{0.9}(\text{MAPbBr}_3)_{0.1}$ single crystal device.....	S11
Figure S11. Relative permittivity of the $(\text{FAPbI}_3)_{0.9}(\text{MAPbBr}_3)_{0.1}$ single crystal device	S12

(a)



(b)

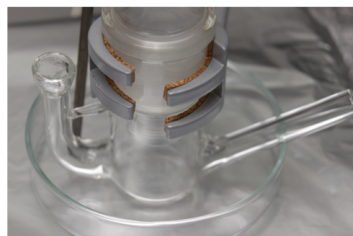


Figure S1. (a) Setup of RFCM. (b) Custom-made vessel with two glass tubes for $(\text{FAPbI}_3)_{0.9}(\text{MAPbBr}_3)$ single crystal growth.

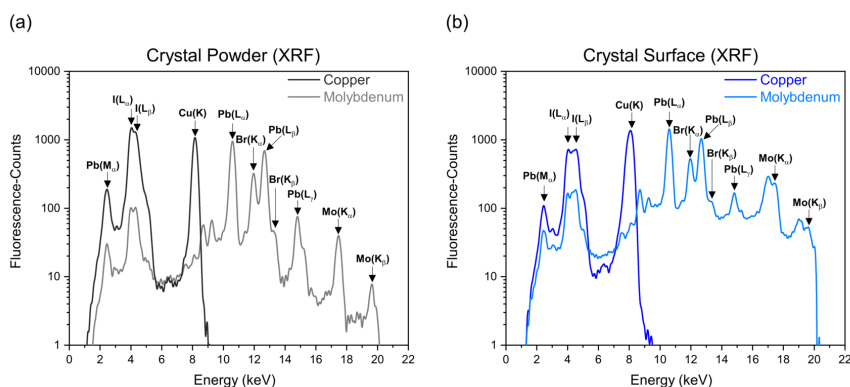


Figure S2. XRF results of the $(\text{FAPbI}_3)_{0.9}(\text{MAPbBr}_3)_{0.1}$ crystal powder (a) and (b) the crystal surface to qualitatively determine the incorporation of the elements Br, I and Pb using an unfiltered Mo- $\text{K}\alpha$ and a Cu- $\text{K}\alpha_1$ radiation source, respectively.

Table S1. Evaluation of the XRF measurements, presented by energies of principal K-, L-, and M-shell emission lines of Br, I and Pb.

Emission Line		Theory ¹ (keV)	Experimental Data ² (keV)	
			Powder	Surface
Bromine	K α_1	11.92	12.0	12.0
	K α_2	11.88		
	K β_1	13.29	13.3	13.3
	L α_1	1.48		
	L α_2	1.48		
	L β_1	1.53		
Iodine	K α_1	28.61		
	K α_2	28.32		
	K β_1	32.29		
	L α_1	3.94	4.0	4.0
	L α_2	3.93		
	L β_1	4.22	4.3	4.3
	L β_2	4.51		4.6
L γ_1	4.80	5.0	5.0	
Lead	K α_1	74.97		
	K α_2	72.80		
	K β_1	84.94		
	L α_1	10.55	10.6	10.6
	L α_2	10.45		
	L β_1	12.61	12.7	12.7
	L β_2	12.62		
	L γ_1	14.76	14.8	14.8
	M α_1	2.35	2.4	2.4

¹ J. Kirz, D. Attwood, B. Henke, M. Howells, K. Kennedy, K. Kim, J. Kortright, R. Perera, P. Pianetta, J. Riordan, J. Scofield, G. Stradling, A. Thompson, J. Underwood, D. Vaughan, G. Williams and H. Winick, in *Center for X-ray Optics, X-ray Data Booklet*, ed. D. Vaughan, Lawrence Berkeley Laboratory/ University of California, Berkeley, 1985, chapter 2.3, pages 14, 15, 17.

² The collected data were determined by the peak maximum and have an accuracy of ± 0.1 keV.

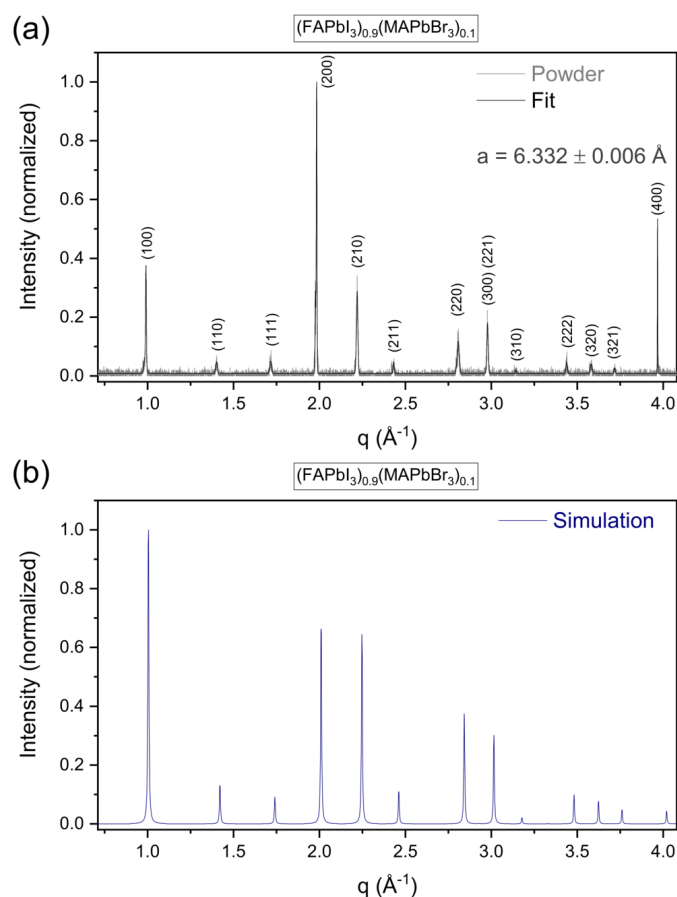


Figure S3. (a) Measured XRD pattern of the $(\text{FAPbI}_3)_{0.9}(\text{MAPbBr}_3)_{0.1}$ crystal powder with associated fit. (b) Simulated³ XRD pattern indicating a simple cubic system.

Table S2. Evaluation of the XRD fitting data of the $(\text{FAPbI}_3)_{0.9}(\text{MAPbBr}_3)_{0.1}$ crystal powder to determine the lattice plane d_{hkl} and the lattice constant a .

Number	Fitting Data q (\AA^{-1})	Miller Indices (hkl)	d_{hkl} (\AA)	a (\AA)
1	0.9907 ± 0.000038	100	6.341	6.341
2	1.4013 ± 0.000446	110	4.484	6.341
3	1.7165 ± 0.000461	111	3.661	6.340
4	1.9833 ± 0.000014	200	3.168	6.336
5	2.2193 ± 0.000060	210	2.831	6.331
6	2.4317 ± 0.000383	211	2.584	6.329
7	2.8071 ± 0.000178	220	2.238	6.331
8	2.9778 ± 0.000091	221	2.110	6.330
9	3.1421 ± 0.000886	310	1.600	6.323
10	3.4373 ± 0.000428	222	1.828	6.332
11	3.5803 ± 0.000589	320	1.755	6.328
12	3.7176 ± 0.000885	321	1.690	6.324
13	3.9667 ± 0.000015	400	1.584	6.336

³ L. Chen, Y.-Y. Tan, Z.-X. Chen, T. Wang, S. Hu, Z.-A. Nan, L.-Q. Xie, Y. Hui, J.-X. Huang, C. Zhan, S.-H. Wang, J.-Z. Zhou, J.-W. Yan, B.-W. Mao and Z.-Q. Tian, *Journal of the American Chemical Society*, 2019, DOI: 10.1021/jacs.8b11610.

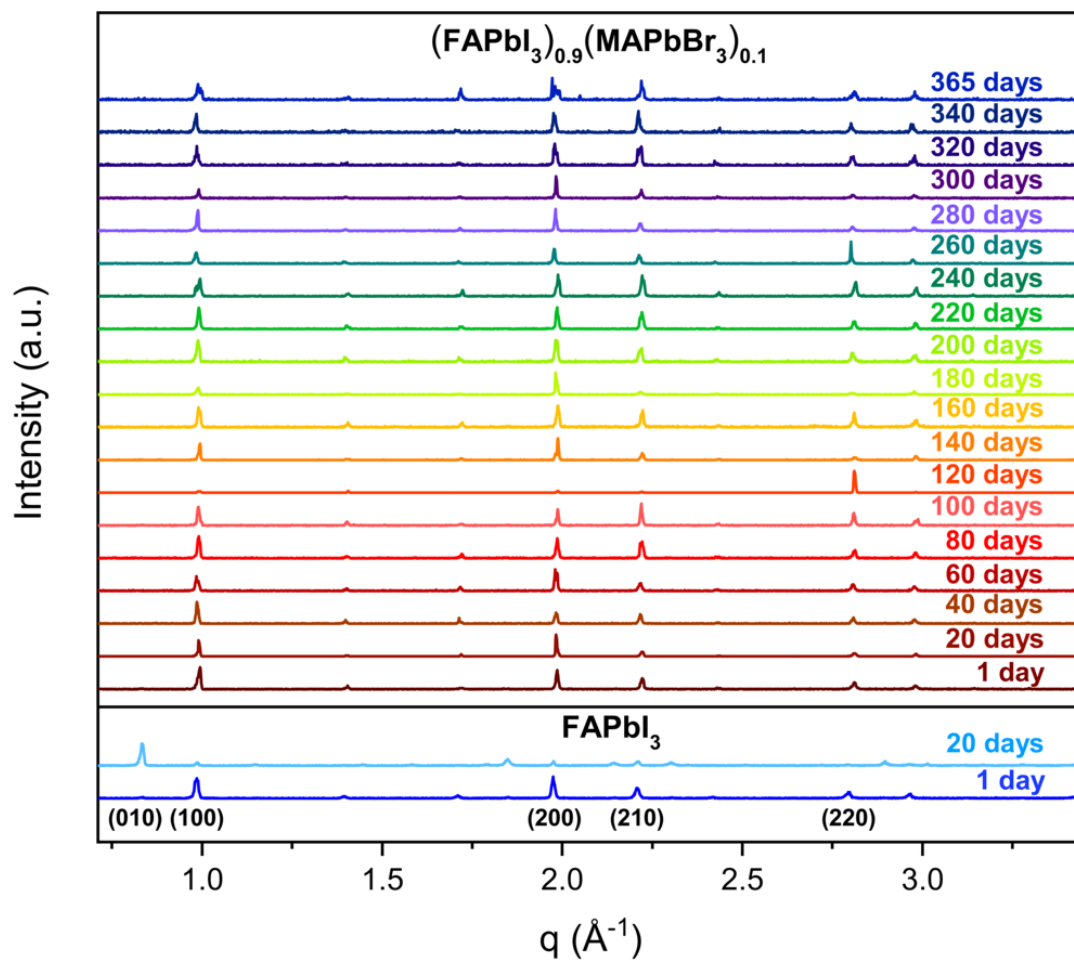


Figure S4. Long-term stability XRD – test over one year of the $(\text{FAPbI}_3)_{0.9}(\text{MAPbBr}_3)_{0.1}$ crystal powder. Compared to the FAPbI_3 crystal powder, the double cation – double halide perovskite powder is stable under ambient conditions. The δ -peak (010), an indication of decomposed crystal powder, is only observed by the spectrum of the FAPbI_3 crystal powder.

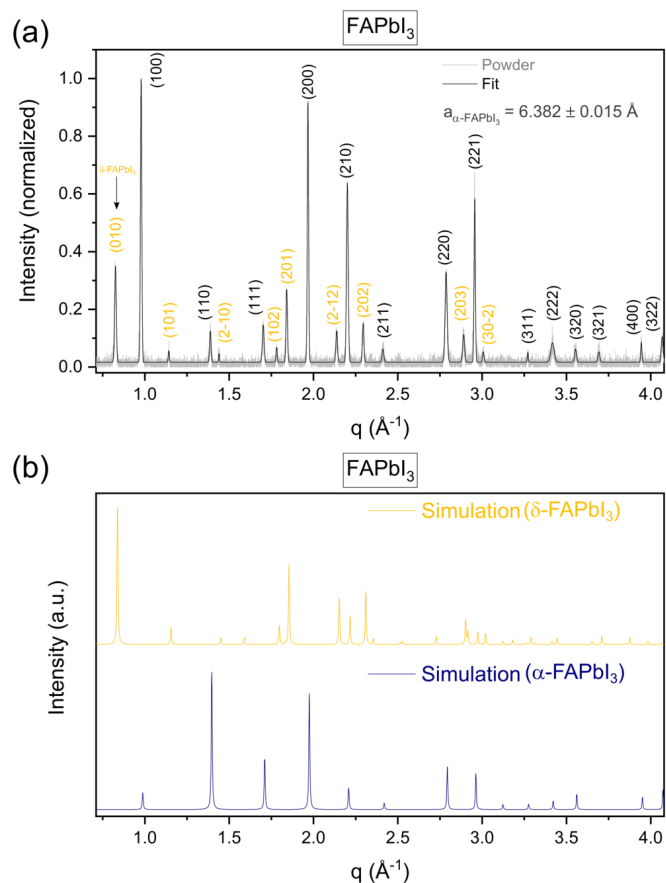


Figure S5. (a) Measured XRD pattern of the FAPbI₃ crystal powder with associated fit. (b) Simulated^{4,5} XRD patterns of the α - and δ -phase of FAPbI₃.

Table S3. Evaluation of the XRD fitting data to determine the lattice plane d_{hkl} and the lattice constant a of the α -FAPbI₃ crystal powder.

Number	Fitting Data q (\AA^{-1})	Miller Indices (hkl)	d_{hkl} (\AA)	a (\AA)
1	0.9782 ± 0.000025	100	6.423	6.423
2	1.3885 ± 0.000227	110	4.5251	6.400
3	1.7020 ± 0.000208	111	3.6916	6.394
4	1.9673 ± 0.000025	200	3.1938	6.388
5	2.2009 ± 0.000042	210	2.8548	6.384
6	2.4115 ± 0.000598	211	2.6055	6.382
7	2.7864 ± 0.000092	220	2.2549	6.378
8	2.9560 ± 0.000040	221	2.1256	6.377
9	3.2706 ± 0.000580	310	1.9211	6.372
10	3.4172 ± 0.000537	222	1.8387	6.369
11	3.5539 ± 0.000590	320	1.7680	6.375
12	3.6921 ± 0.000741	321	1.7018	6.368
13	3.9440 ± 0.000306	400	1.5931	6.372
13	3.9646 ± 0.000475	321	1.585	5.930

⁴ A. A. Zhumekenov, M. I. Saidaminov, M. A. Haque, E. Alarousu, S. P. Sarmah, B. Murali, I. Dursun, X.-H. Miao, A. L. Abdelhady, T. Wu, O. F. Mohammed and O. M. Bakr, *ACS Energy Letters*, 2016, **1**, 32-37.

⁵ M. T. Weller, O. J. Weber, J. M. Frost and A. Walsh, *The Journal of Physical Chemistry Letters*, 2015, **6**, 3209-3212.

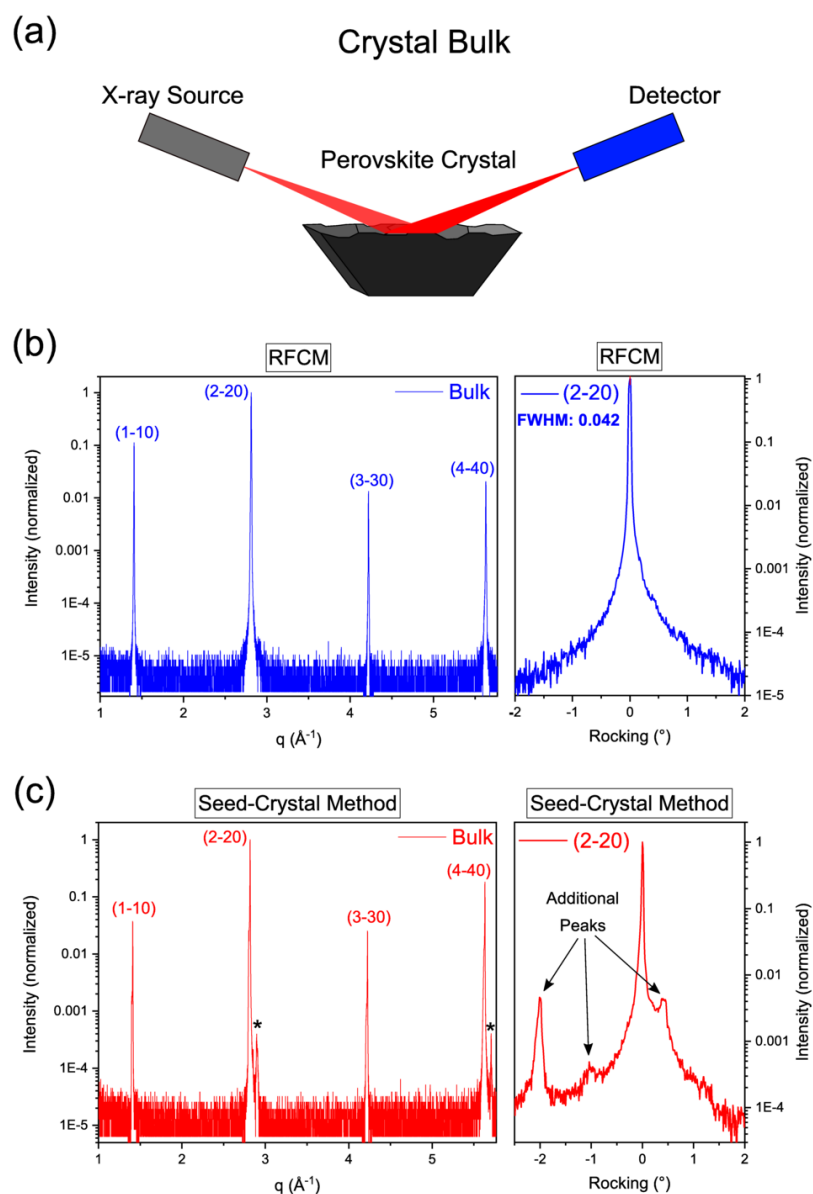


Figure S6. (a) Comparison of out-of-plane XRD bulk measurements and corresponding (2-20) rocking scans (b) of a single crystal and (c) of a crystal grown with a seed crystal. The crystals were cut along the [110] direction with a scalpel to measure the centre of the crystal. Additional “*” signed peaks can be associated to further Bragg reflexes.

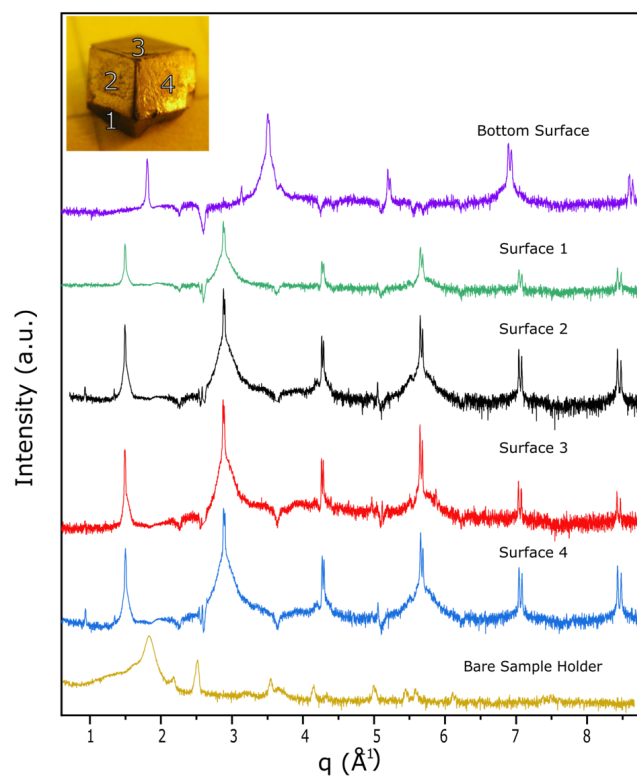


Figure S7. Bare sample holder data and subtracted XRD data in reflection geometry, recorded from different surfaces of a $(\text{FAPbI}_3)_{0.9}(\text{MAPbBr}_3)_{0.1}$ single crystal. (Inset: crystal image with corresponding surfaces numbers.)

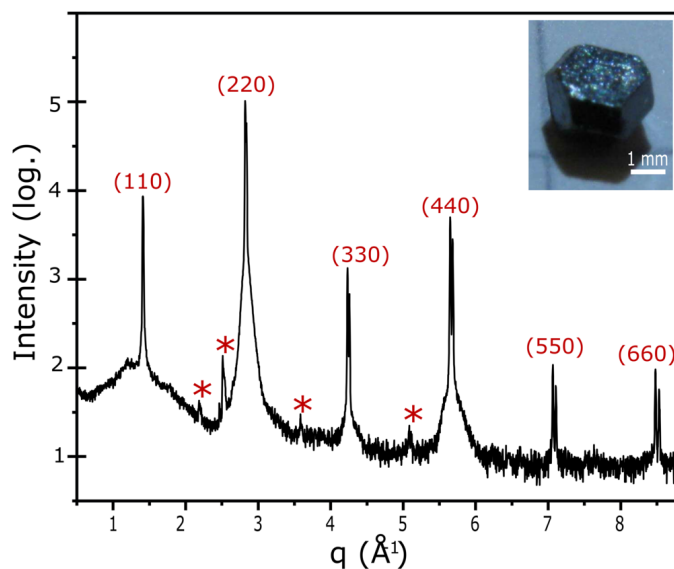


Figure S8. X-ray Bragg scattering intensities in reflection geometry of a $(\text{FAPbI}_3)_{0.9}(\text{MAPbBr}_3)_{0.1}$ single crystal. Insets: photograph of the single crystal. Additional "*" signed peaks could be corresponded to the lead tape of the sample holder. Furthermore, amorphous background scattering at about $1 - 2 \text{\AA}^{-1}$ is observed, which can be associated with the Kapton tape.

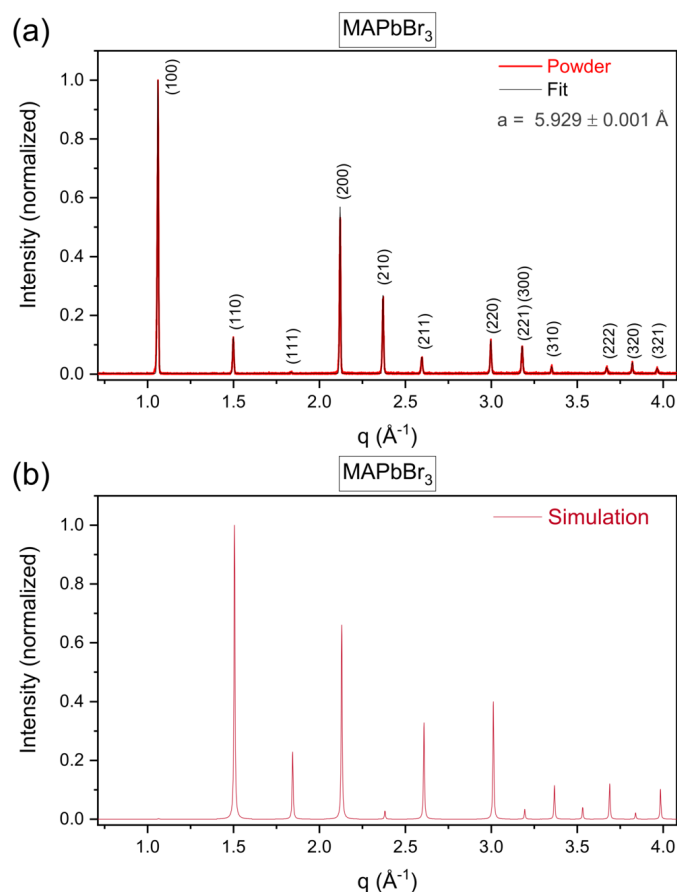


Figure S9. (a) Measured XRD pattern of the MAPbBr₃ crystal powder with associated fit. (b) Simulated⁶ XRD pattern indicating a simple cubic system.

Table S4. Evaluation of the XRD fitting data to determine the lattice plane d_{hkl} and the lattice constant a of the MAPbBr₃ crystal powder.

Number	Fitting Data q (\AA^{-1})	Miller Indices (hkl)	d_{hkl} (\AA)	a (\AA)
1	1.0604 ± 0.000078	100	5.926	5.926
2	1.4987 ± 0.000065	110	4.192	5.929
3	1.8360 ± 0.002069	111	3.422	5.928
4	2.1200 ± 0.000013	200	2.964	5.928
5	2.3697 ± 0.000030	210	2.652	5.929
6	2.5957 ± 0.000151	211	2.421	5.929
7	2.9968 ± 0.000071	220	2.097	5.930
8	3.1791 ± 0.000089	221	1.976	5.929
9	3.1791 ± 0.000089	300	1.976	5.929
10	3.3507 ± 0.000332	310	1.875	5.929
11	3.6714 ± 0.000422	222	1.712	5.929
12	3.8199 ± 0.000193	320	1.645	5.930

⁶ A. Poglitsch and D. Weber, *The Journal of Chemical Physics*, 1987, **87**, 6373-6378.

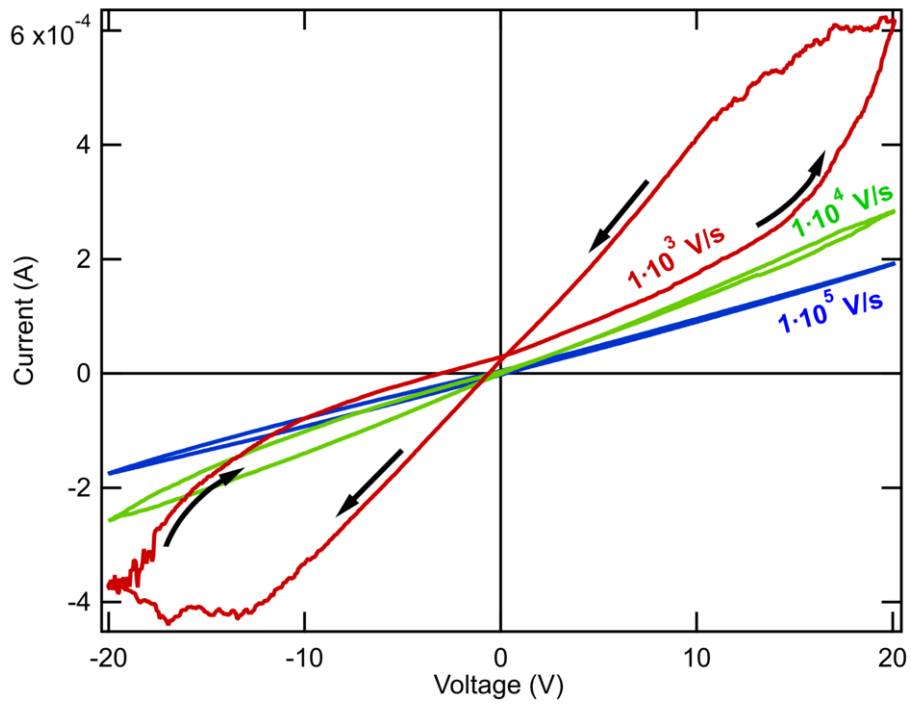


Figure S10. I-V curves with hysteresis loops of the $(\text{FAPbI}_3)_{0.9}(\text{MAPbBr}_3)_{0.1}$ single crystal device with the geometry of a plate capacitor. The same single crystal device was used as previously for the determination of relative permittivity and AC electrical conductivity. The measurements were carried out at room temperature.

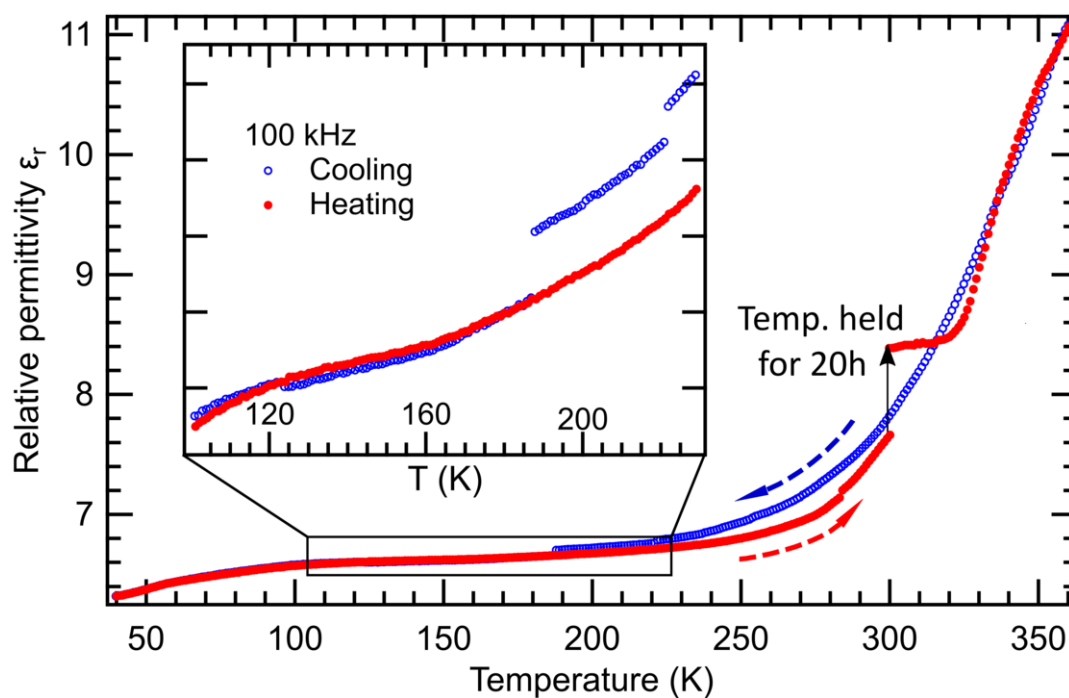


Figure S11. Relative permittivity of the $(\text{FAPbI}_3)_{0.9}(\text{MAPbBr}_3)_{0.1}$ single crystal device. Jumps are visible during the successive temperature cycles with 0.7 K min^{-1} .

During the heat up-cycle, the sample was kept at 300 K for 20 h before it was heated further to 360 K. This led to a jump in the measured dielectric constant, indicating a slow response to the applied temperature. The visible discontinuities below 300 K could indicate phase transitions in a single crystal system where they cannot occur gradually in individual grains, as found by Cordero et al. in pressed FAPbI_3 powder⁷, but they are too small to exclude artefacts.

⁷ F. Cordero, F. Craciun, F. Trequattrini, A. Generosi, B. Paci, A. M. Paoletti and G. Pennesi, *The Journal of Physical Chemistry Letters*, 2019, **10**, 2463-2469.